



Cite this: DOI: 10.1039/c6nj00409a

Heteroleptic Cu(II)–polypyridyl complexes as photonucleases†‡

V. Singh,^{ab} K. Sharma,^a B. Shankar,^a S. K. Awasthi^a and R. D. Gupta^{*c}

A series of heteroleptic Cu(II)–polypyridyl complexes with terpyridine (3N)/imidazole (2N) backbones and appended with pyridyl, 2-naphthyl, 9-anthryl and 1-pyrenyl groups are synthesized and evaluated for their photonuclease activity. An array of techniques *viz.* UV-vis, fluorescence, circular dichroism and thermal denaturation established strong DNA binding affinity ($K_b = \sim 10^4\text{--}10^6\text{ M}^{-1}$) and the binding modes were correlated with molecular docking studies. Photonuclease efficiency exceeded 90% for all the complexes under identical conditions. Interestingly, DNA binding propensity and photonuclease efficiency followed the increasing size, planarity, aromaticity, π -Stacking ability and hydrophobicity of the peripheral moiety.

Received (in Victoria, Australia)
6th February 2016,
Accepted 5th May 2016

DOI: 10.1039/c6nj00409a

www.rsc.org/njc

Introduction

The stability of deoxyribonucleic acid (DNA) against potential nucleophiles^{1,2} sustains biological life, while *in vivo* DNA cleavage forms the basis of replication and transcription processes.^{3–6} In this context, the manipulation of DNA with small molecules could be useful in biotechnology,^{7–9} medicine¹⁰ and cancer therapy.^{11,12} In particular, phthalocyanine and porphyrin-based compounds are proven to have strong photo-nuclease activity^{13–15} but are known to cause severe side effects.¹⁶ Metal-based nucleases, such as cisplatin, are a huge success but are non-specific in action and lose effectiveness, in the long run, owing to covalent interactions with DNA. At present, much research is focused on developing metal-based photonucleases, operating through non-covalent interactions, as these can impart structural, optical and electronic advantages, along with energetic contributions to their interactions with anionic DNA.^{17–19}

Therefore, and in this direction, a series of heteroleptic Cu(II)–polypyridyl complexes are tested for their chemical as well as photo-nuclease activity. These nucleases utilize a terpyridine/imidazole spine (Fig. 1) for coordinating to a copper center,

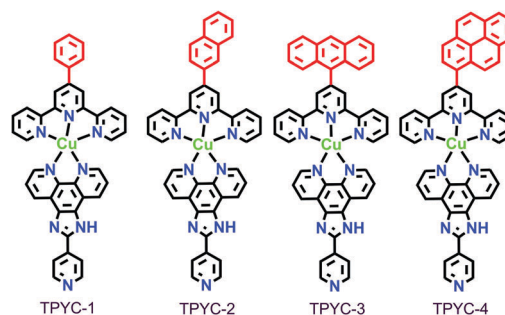


Fig. 1 Representation of Cu(II)–polypyridyl complexes, TPYC-1 to TPYC-4, where TPYC-1 = pyridyl; TPYC-2 = 2-naphthyl; TPYC-3 = 9-anthryl and TPYC-4 = pyrenyl-appended complexes (see the red part), respectively.

while functionalized pyridyl, naphthyl, anthryl and pyrenyl act as active front-intercalators. Importantly, the ligand architecture ensures a lower electron density at the metal centre, which allows improved interaction with the anionic DNA, as confirmed by density functional studies. This design strategy led to comparatively high DNA binding affinities through non-covalent interactions, while proposed DNA binding modes were correlated with molecular docking studies. Significantly, experimental as well as theoretical evidence categorically suggested that DNA binding and photocleavage follow the intrinsic properties of the peripheral moieties.

Results and discussions

Synthesis and characterization

Fig. 1 illustrate the ligand architecture (TPY-1 to 4; terpyridyl-based ligand and IMI-1; imidazole-based ligand) and the corresponding Cu(II)–polypyridyl complexes (TPYC-1 to 4).

^a Department of Chemistry, University of Delhi, Delhi-110 007, India

^b Department of Chemical Engineering, Pohang University of Science and Technology, Pohang-790-784, South Korea

^c Faculty of Life Sciences and Biotechnology, South Asian University, Delhi-110 021, India. E-mail: rdgupta@sau.ac.in

† Dedicated to Late Dr Tarkeshwar Gupta.

‡ Electronic supplementary information (ESI) available: Synthesis of ligands (TPY-1 to 4 and IMI-1); ¹H NMR spectra of TPY-1 to 4; ESI-MS spectra of complexes TPYC-1 to 4; details of UV-vis studies, competitive displacement assay, circular dichroism studies, thermal denaturation studies, chemical and photo-nuclease activity and mechanistic experiments; Tables S1 and S2; Fig. S1–S16. See DOI: 10.1039/c6nj00409a

Table 1 Selected physicochemical data for complexes TPYC-1 to 4

TPYC	IR ^a /cm ⁻¹ [ν (ClO ₄ ⁻)]	λ _{max} /nm (log ε/M ⁻¹ cm ⁻¹)	E _{1/2} /V (ΔE _p /V) ^d	I _{pa} /I _{pc} (D/cm ² s ⁻¹)
1	1076	744 (1.81) ^b	0.0280 (0.34)	0.25 (2.8 × 10 ⁻⁴)
2	1082	607 (2.36) ^c	0.0025 (0.36)	0.86 (8.4 × 10 ⁻⁴)
3	1079	671 (1.73) ^c	0.0075 (0.41)	0.40 (1.0 × 10 ⁻⁴)
4	1092	594 (1.84) ^c	-0.35 ^e (NA)	NA (5.0 × 10 ⁻⁵)

^a ATR-IR using ZnSe crystal. ^b In 10% DMF, ligand field bands. ^c In CH₃CN. ^d Redox couple (Cu²⁺/Cu⁺) in 30% aqueous DMF-0.1 mM TBAP, E_{1/2} = 0.5(E_{pa} + E_{pc}), ΔE_p = (E_{pa} - E_{pc}), where E_{pa} and E_{pc} are the anodic and cathodic peak potentials, respectively. The potentials are vs. Ag/AgCl. Scan rate = 0.4 V s⁻¹. ^e E_{pc} (NA = not available).

In a typical synthesis procedure for TPYC-1 to 4, 74 mg (0.02 mmol) Cu(ClO₄)₂·6H₂O was dissolved in 10 mL MeOH/CHCl₃ (1:1, v/v) at room temperature. To the stirred solution, 0.02 mmol of the respective TPY ligand in 10 mL MeOH/CHCl₃ (1:4, v/v) was added dropwise. The solution was stirred for 2 h and then 59.4 mg (0.02 mmol) IMI-1 in 10 mL MeOH/CHCl₃ (4:1, v/v) was added dropwise to the stirred solution. Further stirring for 1 h afforded a light to dark green coloured precipitate. The precipitate was washed with ether, dried over anhydrous calcium chloride and kept in a glovebox. Average yield: ~40–55%. Detailed synthetic procedures and characterizations are provided in the ESI† (see Fig. S1–S9 and Table 1). The following sub-sections will provide detailed UV-vis absorption, electrochemical, and electron paramagnetic resonance characteristics, as well as DNA binding and cleavage studies of these complexes, including molecular docking studies.

UV-vis absorption characteristics. The UV-vis spectra of heteroleptic, penta-coordinated, 3d⁹ Cu(II)-complexes (see Fig. S10, ESI†; Table 1) exhibited ligand-centred bands due to spin-allowed π → π* or n → π* transitions in the UV and the near UV region. Additionally, characteristically broad and relatively weak metal-centred or d → d bands appeared, as signified by their log ε values (see Table 1). These ligand field bands are intrinsically short-lived because they involve the population of the strongly metal–ligand antibonding orbital, usually designated as the d_{z²-y²} orbital at the higher wavelengths (λ_{max} > 600 nm). Similar d → d transitions have been observed for such penta-coordinated Cu(II)-complexes and have been attributed to the symmetry-allowed ²B₁ → ²E transition, which points to the square-pyramidal geometry of these complexes.²⁰ We further used the UV-vis technique to assess the stability of the complexes in 10% DMF/tris-HCl buffer solutions and found them to be stable for ~1 week as there were no observable changes in their respective UV-vis spectra during this period (see Fig. S11, ESI†).

Electrochemical characteristics. Cyclic voltammograms of TPYC-1 to 4 were recorded in 10% DMF/tris-HCl buffer solution and showed quasi-reversibility features (see Fig. 2; Table 1), that is, the reduction half-wave is not entirely reproduced during the oxidation process, as corroborated by the ratio of anodic to cathodic current (I_{pa}/I_{pc}) values. For these complexes, the Cu^{2+/+} couple was observed at a cathodic peak potential, E_{pc} ~ -0.14 V to -0.35 V (vs. Ag/AgCl) with large ΔE_p values ranging from 0.34 V to 0.41 V at a scan rate of 100 mV s⁻¹ and half-wave redox

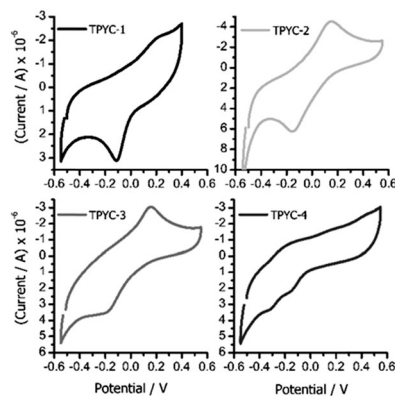


Fig. 2 Cyclic voltammograms of copper complexes in 10% DMF (1 mM) and TBAP as supporting electrolyte (0.1 mM) vs. Ag–AgCl at a scan rate of 100 mV s⁻¹.

potential, E_{1/2} values close to 0.02 V, with no anodic response in the case of TPYC-4. An increasing trend was seen in ΔE_p values with concomitant large negative values of E_{pc} on increasing the scan rate from 100 to 1000 mV s⁻¹ (Fig. S12, ESI†), which could be attributed to the increasing size of the aromatic tail units and their electron donating ability. These factors stabilize the Cu²⁺ oxidation state and make Cu²⁺ → Cu⁺ conversion less feasible thermodynamically. Moreover, the observed cathodic and anodic shifts with increasing scan rate implied non-Nernstian behaviour, possibly attributed to heterogeneous electron transfer kinetics and coupled chemical reaction(s).²¹ The plot of cathodic peak current vs. the square root of the scan rate (I_{pc} vs. ν^{1/2}) for each of the complexes gives linear fitting (R² ~ 0.97 to 0.99) and is indicative of a diffusion-controlled process (Fig. S13, ESI†). The slope of each I_{pc} vs. ν^{1/2} plot is calculated, and the diffusion constant, D (see Table 1) is calculated using the Randles–Sevcik equation for diffusion-controlled electrochemical processes.²²

EPR characteristics. EPR spectra for the complexes presented an oblate axial with g_{||} > g_⊥ > g_e and a d_{x²-y²} ground state, that is, an unpaired electron resides in the d_{x²-y²} orbital and displays a typical four-line spectrum (three well-resolved and one overlapped with the g_⊥ signal (Fig. 3 and Fig. S14, ESI†)). For all complexes, g_{||} values are around 2.18, which signifies that Cu²⁺ is coordinated to N-atoms in a square pyramidal geometry as coordination through O-atoms (possibly through H₂O or the perchlorate moiety), which would have resulted in larger g_{||} values (see Table S1, ESI†). Moreover, trigonal bipyramidal geometry (tbp) is not feasible, as the g_{||} < g_⊥ condition must have been satisfied.²³

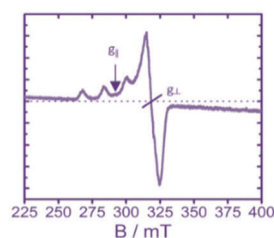


Fig. 3 X-band EPR spectrum of complex TPYC-1 in DMF glass at 77 K. (frequency 9.1 GHz and 100 kHz field).

G values in the range 3–4 further confirm the square-based geometries of these complexes, which are retained in the solution phase and allow for small exchange coupling.²⁴ Hyperfine coupling constant, A_{\parallel} values are $\geq 160 \times 10^{-4} \text{ cm}^{-1}$ for all the complexes, which is expected for a square-based CuN_5 chromophore.²⁵ The degree of distortion, $f(x) = (g_{\parallel}/A_{\parallel})$, is considered as an index of deviation from the idealized geometry.^{26,27} For planar complexes, $g_{\parallel}/A_{\parallel}$ has values ranging from 110 to 120 cm^{-1} , while 130–150 cm^{-1} indicates slight to moderate distortion and 180–250 cm^{-1} indicates considerable distortion from the ideal geometry. For the complexes studied, $g_{\parallel}/A_{\parallel}$ values are in the range 120 to 140, which indicates slight to moderate distortions from the square-based geometry;²⁸ g_{\parallel} values < 2.3 are indicative of covalent bonding in these complexes.²⁹ Kivelson and Nieman suggested an equation for calculating the in-plane σ -covalency parameter (α^2) (see eqn (1)).³⁰

$$\alpha^2 = |A_{\parallel}/P| + (g_{\parallel} - 2.0023) + 3/7(g_{\perp} - 2.0023) + 0.04 \quad (1)$$

where ' P ' is the dipolar hyperfine coupling parameter (-0.036 cm^{-1}). The values of α^2 lie between 0.5 and 1, the limits of pure covalent and pure ionic bonding, respectively. For these complexes, α^2 lies in the range 0.67 to 0.74, which accounts for the fraction of the unpaired electron density located on Cu^{2+} and is indicative of considerable covalency in the σ -bond.^{28–31}

DNA binding, molecular docking, chemical and photonuclease activities

DNA binding. Complexes TPYC-1 to 4 showed quite similar behaviour during absorption spectral titrations (AST) with ct-DNA (see ESI† for experimental details). Perturbations in ligand-centred bands were monitored during the addition of ct-DNA, where all complexes showed varying degrees of hypochromism (~ 12 to 40%), accompanied by minor to significant red shifts (~ 1 to 8 nm) in the respective absorption bands of their UV-vis spectra, mostly ligand-centred bands (see Fig. 4, Table 2 and Fig. S15, ESI†). These features were strongly suggestive of non-covalent binding of complexes with DNA. The appearance of isosbestic points indicated two absorbing species, *viz.* complex and DNA, linearly related by stoichiometry, although ratios of more than 1 : 1 are possible. Moreover, uncoordinated $-\text{NH}$ groups of the imidazole moiety and N-atoms of the pyridyl moiety could possibly allow secondary interactions, such as hydrogen bonding with DNA, which possesses several hydrogen bonding sites accessible both in the minor and major grooves. This is supported by low bathochromic shifts in the case of TPYC-1 and higher ones for TPYC-3 and TPYC-4. Intrinsic binding constants, K_b ($\sim 10^4 - 10^6 \text{ M}^{-1}$; see Table 2), values suggested strong and increasing DNA binding affinity from TPYC-1 to TPYC-4 and are thus consistent with the intercalative binding mode.

Competitive displacement assays using ethidium bromide (EB) (see ESI† for experimental details) complement UV-vis studies (Fig. 5A and Fig. S16 and S17, ESI†). Apparent binding constant, K_{app} values followed the same order as for K_b . Additionally, DC_{50} , the concentration of the complex at 50% EB displacement, values for TPYC-3 and TPYC-4 were significantly low at $\sim 2 \mu\text{M}$ and are in line with structural characteristics of ancillary ligands

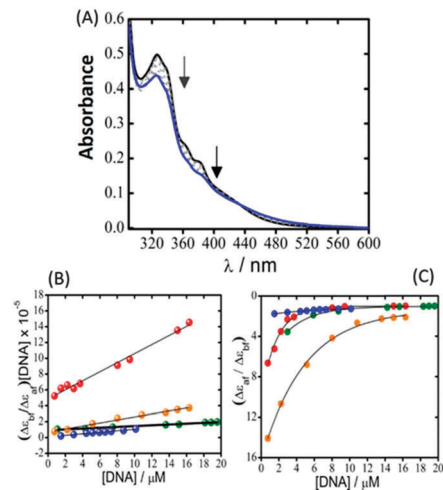


Fig. 4 Representative example showing (A) spectral traces of TPYC-3 (10 μM) in 10% DMF upon gradual addition of ct-DNA (300 μM) in 50 mM tris-HCl buffer; (B) non-linear least-squares fitted plot of $\Delta\epsilon_{\text{ar}}/\Delta\epsilon_{\text{bf}} \times [\text{DNA}]$ vs. $[\text{DNA}]$ for all complexes (Red sphere, TPYC-1, $R^2 = 0.98$; Olive sphere, TPYC-2, $R^2 = 0.98$; Orange sphere, TPYC-3, $R^2 = 0.99$; Blue sphere, TPYC-4, $R^2 = 0.99$) using MvH equation; (C) linear least-squares fitted plot $\Delta\epsilon_{\text{ar}}/\Delta\epsilon_{\text{bf}}$ vs. $[\text{DNA}]$ (Red circles, TPYC-1, $R^2 = 0.99$; Olive circles, TPYC-2, $R^2 = 0.99$; Orange circles, TPYC-3, $R^2 = 0.99$; Blue circles, TPYC-4, $R^2 = 0.99$) using modified McGhee von Hippel equation given by Bard and co-workers.

(see Fig. 5B and Table 2). Furthermore, Stern-Volmer plots showed linear dependencies (see Fig. 5C), which indicated one dominant quenching mechanism, while accessibility to EB-DNA sites increased from TPYC-1 to TPYC-4, as suggested by increasing K_{SV} values. Furthermore, $(K_{\text{SV}})^{-1}$ suggests that anthryl and pyrenyl-terminated complexes can more easily displace EB from EB-DNA sites as larger concentrations of other complexes are required to induce a similar effect (see Table 2).

In thermal denaturation studies, the ct-DNA melting point, T_m^0 , in the presence of TPYC-1 to 4, showed a change (ΔT) of +2.8 to +7.2 $^\circ\text{C}$, where ΔT was found to be highest for TPYC-4 (see Fig. 5D, E and Table 2). In the light of the ΔT values, it could be suggested that these complexes tend to prefer groove/partial intercalation binding modes and play a more significant role in ds-DNA stabilization than simple mono-intercalation.³² Notably, the effect is more pronounced for 'G-C'-rich regions of TPYC-3 and TPYC-4, as is evident from the denaturation curves.³³ Moreover, it can also be noted that ΔT values are not significantly large, implying that covalent interactions with DNA are not a feasible option.³⁴

Circular dichroism experiments produced noticeable changes in the ellipticity of ct-DNA on complex addition (see Fig. 5F). Visible red/blue shifts were observed with respect to the positive band. TPYC-1 and TPYC-2 witnessed +36% and +34% changes in ellipticity along with a minor red shift. For TPYC-3 and TPYC-4, parallel changes in ellipticity were of negative order, that is, -30% and -40% , along with pronounced blue shifts in the positive band. For all complexes except TPYC-4, a negative band exhibited an increase in the intensity. The variations in the CD spectra of ct-DNA with the addition of small molecules are suggestive of

Table 2 Comparative chart for absorption spectral titrations of TPYC-1 to 4 (10 μM) against ct-DNA (300 μM) in 50 mM tris-HCl buffer; competitive binding and thermal denaturation studies

TPYC	$K_b/M^{-1}{}^a$ (s, Γ_{max})	$K_{\text{app}}/M^{-1}{}^b$ ($\text{DC}_{50}/\mu\text{M}$)	K_{SV}^c (K_{SV}^{-1})	$\Delta T_m^d/^\circ\text{C}$
1	$1.80 \pm 0.20 \times 10^4$ (0.119, 4.20)	$1.94 \pm 0.35 \times 10^6$ (6.70 ± 0.22)	1.50 (0.66)	+2.8
2	$1.23 \pm 0.15 \times 10^5$ (0.116, 4.31)	$1.39 \pm 0.20 \times 10^6$ (9.30 ± 0.30)	1.61 (0.62)	+3.2
3	$1.43 \pm 0.24 \times 10^5$ (0.121, 4.13)	$2.71 \pm 0.30 \times 10^6$ (4.80 ± 0.12)	3.60 (0.27)	+4.8
4	$1.05 \pm 0.10 \times 10^6$ (0.125, 4.000)	$7.70 \pm 0.15 \times 10^6$ (1.68 ± 0.25)	11.06 (0.09)	+7.2

^a Intrinsic binding constant. ^b Apparent binding constant. ^c Stern–Volmer quenching constant. ^d Change in DNA melting point.

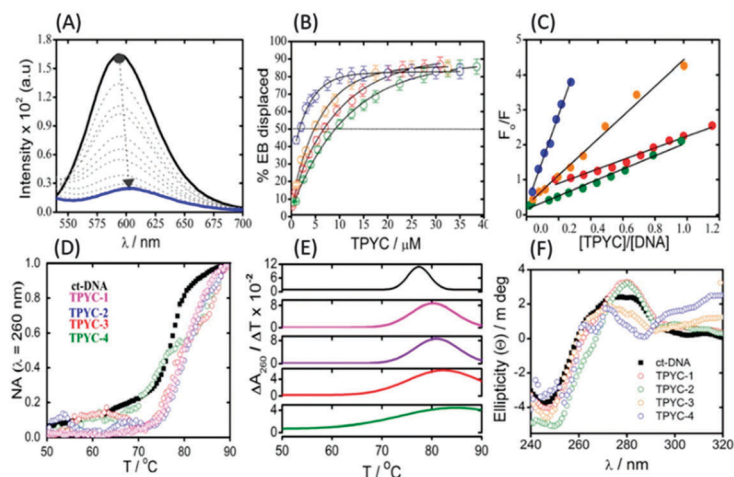


Fig. 5 Top: (A) Representative example of addition of complex (TPYC-3) to EB-bound DNA solution; (B) plot of percent displacement of EB from DNA on gradual addition of complexes (red circles, TPYC-1, $R^2 = 0.99$; olive circles, TPYC-2, $R^2 = 0.99$; orange circles, TPYC-3, $R^2 = 0.99$; blue circles, TPYC-4, $R^2 = 0.99$); (C) Stern–Volmer plots for calculation of quenching constants (red circles, TPYC-1, $R^2 = 0.97$; olive circles, TPYC-2, $R^2 = 0.98$; orange circles, TPYC-3, $R^2 = 0.98$; blue circles, TPYC-4, $R^2 = 0.99$). Bottom (D) DNA melting curves for ct-DNA alone (130 μM) and DNA + complexes TPYC-1 to 4 (33 μM); NA = normalized absorbance; (E) first derivative of DNA melting curves for calculation of T_m ; (F) circular dichroism spectra of DNA alone (100 μM , black line) in 50 mM tris HCl buffer and in the presence of complex solutions (10 μM , coloured circles).

subtle changes in the DNA double helix promoted by stabilization of its secondary structure upon DNA–metal complex interaction, which could be due to either partial intercalative or groove binding to DNA.^{35–37} However, this evidence cannot be used alone to classify the mode of binding.

DFT and molecular docking studies. A careful analysis of the optimized geometries of TPYC-1 to 4 suggests that pyridyl, naphthyl, anthryl and pyrenyl units are in the plane perpendicular to the terpyridyl unit and that, as suggested by EPR studies, there is distortion from the ideal square-based geometry (see Fig. S18, Table S2 and S3, ESI \ddagger). As confirmed by the DNA binding studies, with an increase in the hydrophobicity, planarity and aromaticity of the appended ligand, the DNA-binding propensity increases. DFT studies indicate that these moieties actually take the whole complex to the DNA binding regions. Moreover, the highest occupied molecular orbital (HOMO) in each case resides/is localized over pyridyl, naphthyl, anthryl and pyrenyl units of the terpyridyl unit. The lowest unoccupied molecular orbital (LUMO) is distributed over the metal centre and the terpyridyl unit for all the complexes. The HOMO–LUMO energy gap is a critical parameter for eventual charge transfer interactions within the molecules.³⁸ The HOMO–LUMO energy gap for TPYC-1 is calculated to be 2.44 eV, for TPYC-2 is 2.27 eV, for TPYC-3 is 1.75 eV and for TPYC-4 is 1.77 eV

(see Fig. 6A). It is interesting to note that the energy gap decreases and that the charge transfer process becomes easier from the pyridyl to pyrenyl tail units and correlates well with the UV-vis data, where LMCT bands shift to lower energy for the anthryl and pyrenyl moieties.

Furthermore, docking experiments were performed in order to find out the chosen binding site, along with the preferred orientation of the ligand inside the DNA minor groove (Fig. 6A and Fig. S19, ESI \ddagger). Computational docking studies were carried out to gain a theoretical insight into the interactions between

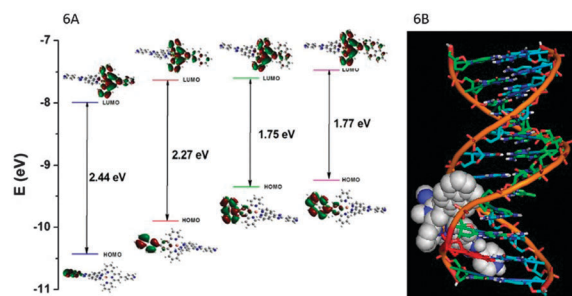


Fig. 6 (A) HOMO–LUMO of TPYC-1 to 4 (left to right) along with energy gap; (B) docked structure of TPYC-4 with d(CGCGAATTCGCG) strands of ct-DNA.

TPYC-1 to 4 and DNA. The optimized structures of the metal complexes were docked with a B-DNA structure (protein data bank; 1BNA) using Autodock 4.2.6. The docked model indicated that TPYC-1 to 4 favoured intercalation into the minor groove of ct-DNA. Structural analysis of the docked structures provided minimum binding energy (BE) values as -36.6 , -34.1 , -35.4 and -46.2 kJ mol^{-1} , respectively, where more negative values indicated more potent binding between DNA and target molecules and correlated well with the experimental evidence; *vide supra*.

Furthermore, we analysed ~ 50 positions for each docked structure. As discussed above, we chose the position that had the highest negative value (minimum energy value). In the case of TPYC-1 and TPYC-4, hydrogen bonding with DNA base pairs was evident (see Fig. 6B) but TPYC-2 and TPYC-3 did not show hydrogen bonding; instead they exhibited van der Waal's interactions with the nearest base pairs. Nonetheless, TPYC-1 is hydrogen-bonded with the guanine 114 (H-bond distance 2.159 Å) of the B chain of DNA, and TPYC-4 with the cyanine 111 (H-bond distance 2.187 Å) of the A chain of DNA (see Fig. 6B). This further supported the strong DNA binding affinity of the complexes.

DNA cleavage activity. For the chemical nuclease activity, the presence of 3-MPA as co-reductant was necessary for pUC19 DNA cleavage as no significant formation of nicked circular DNA ($<4 \pm 2\%$) was observed (see Fig. S20, ESI \ddagger), while due corrections were made for low levels of nicked circular DNA already present.³⁹ This suggested that TPYC-1 to 4 were unable to cleave DNA hydrolytically. Concentration optimization studies revealed that, for all complexes, concentrations as low as ~ 10 μM were able to achieve $>90\%$ cleavage and at ~ 15 μM , DNA cleavage exceeds $\sim 99\%$ with ~ 2 – 3% deviation from the average value (see Fig. 7(left) and 8A).

Furthermore, mechanistic studies (see ESI \ddagger) advocated the involvement of reactive oxygen species (ROSS) in the nuclease activity (see Fig. 7(centre) and 8B). In this connection, there was no effect from the addition of a $^1\text{O}_2$ quencher, NaN_3 (~ 1 – 3% decrease in cleavage activity) or a $^1\text{O}_2$ lifetime enhancer, D_2O (~ 2 – 3% enhancement in cleavage activity), which suggested little or no role of $^1\text{O}_2$ in the cleavage reactions. Moreover, the addition of the hydroxyl radical scavenger, DMSO, reduced the nuclease activity to ~ 5 – 10% , which unambiguously recommended the involvement of hydroxyl radicals in DNA cleavage. The addition

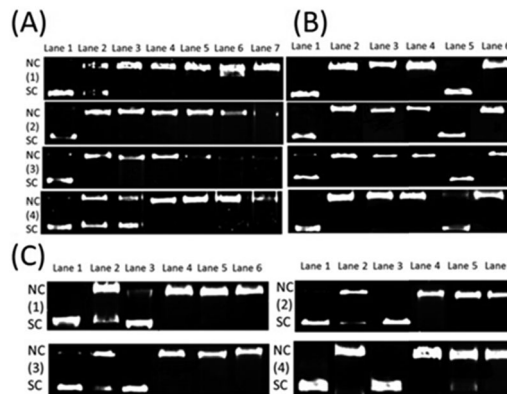


Fig. 8 (A) Gel electrophoresis diagrams showing chemical nuclease activity of TPYC-1 to 4 (1) TPYC-1, (2) TPYC-2, (3) TPYC-3, (4) TPYC-4 with increasing concentration of complexes as we move from lane 2 to lane 7. Lane 1: DNA control (0.5 μL in each case); Lane 2: DNA + 5 μM TPYC + MPA; Lane 3: DNA + 6.67 μM TPYC + MPA; Lane 4: DNA + 8.33 μM TPYC + MPA; Lane 5: DNA + 11.11 μM TPYC + MPA; Lane 6: DNA + 12.22 μM TPYC + MPA; Lane 7: DNA + 13.89 μM TPYC + MPA. (B) Gel electrophoresis diagram showing chemical nuclease activity of TPYC-1 to 4 (10 μM) in the presence of various controls. Lane 1: DNA control (0.5 μL in each case); Lane 2: DNA + TPYC + MPA; Lane 3: DNA + TPYC + MPA + NaN_3 ; Lane 4: DNA + TPYC + MPA + D_2O ; Lane 5: DNA + TPYC + MPA + DMSO; Lane 6: DNA + TPYC + MPA + KI. (C) Gel electrophoresis diagrams of photonuclease activity of complexes TPYC-1 to 4. (1) TPYC-1; (2) TPYC-2; (3) TPYC-3; (4) TPYC-4. Lane 1: DNA control + UV light; Lane 2: DNA + TPYC + UV light; Lane 3: DNA + TPYC + NaN_3 + UV light; Lane 4: DNA + TPYC + D_2O + UV light; Lane 5: DNA + TPYC + DMSO + UV light; Lane 6: DNA + TPYC + KI + UV light.

of KI did not produce any significant variation in the nuclease activity (~ 1 – 3% decline in cleavage activity). Furthermore, the linear form (form III) could not be discerned in any of the chemical nuclease experiments. Therefore, an oxidative cleavage mechanism following type-I processes for DNA cleavage was found to be active for the complexes under study, where Cu^+ , being less stable than Cu^{2+} , most probably helps in reducing molecular oxygen to reactive/reduced oxygen species/intermediates (ROS's), *viz.*, OH^\bullet . Based on literature and experimental evidence, a DNA cleavage mechanism is proposed. At first, copper complexes bind to DNA. Then, 3-MPA reduces the DNA-bound Cu^{2+} to Cu^+ . The H_2O_2 formed oxidizes the DNA-bound Cu^+ -complex to the Cu^{2+} -complex, leading to the formation of OH^\bullet at the binding sites,

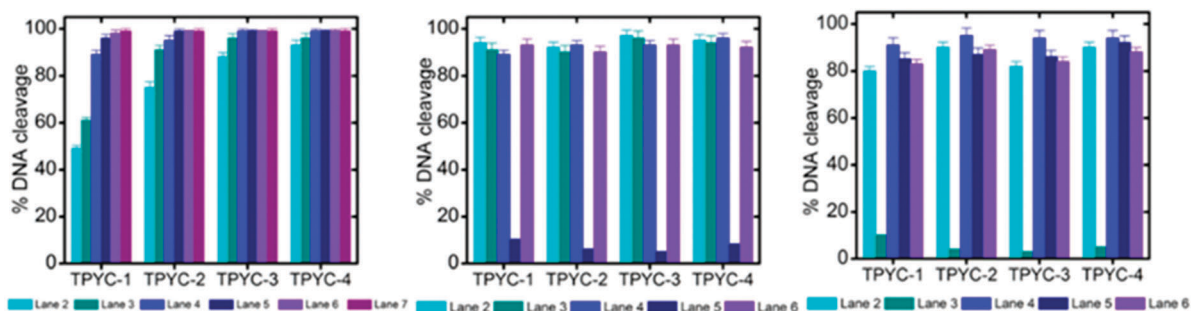


Fig. 7 Bar diagram showing the % DNA cleavage upon treating with complexes TPYC-1 to 4. (left) % DNA cleavage at various concentrations of different complexes. (middle) % DNA cleavage at 10 μM complex and various controls. (right) % DNA cleavage during photonuclease activity of complexes.

thus initiating the chain reaction, which relaxes the supercoiled form to nicked circles (Scheme S1, ESI†).⁴⁰

Photo-exposure of TPYC-1 to 4 + DNA to UV-A light at 365 nm and 12 W power (UV-A source) produced significant nuclease activity as ~80–90% of SC DNA converted to NC DNA within 0.5 h of irradiation (see Fig. 7(right) and 8C). The addition of NaN₃ reduced the cleavage of SC DNA to a mere ~5–10%. In consonance with this, the presence of D₂O enhanced the cleaving activity by up to ~5–12%. The presence of either DMSO or KI did not have any noticeable effect on photonuclease activity. These results were found to be consistent with the formation of ¹O₂ species and further highlighted the necessity of molecular oxygen in photonuclease activities. Mechanistically, UV-A light seemed to sensitize the complexes to an excited state, which upon efficient energy transfer appeared to activate oxygen from its stable triplet (O₂, ³Σ_{g-}) to the highly toxic singlet (O₂, ¹Δ_g) state and thus followed type II processes for effecting DNA cleavage (Scheme S2, ESI†).²²

Conclusions

The heteroleptic copper(II)–polypyridyl complexes were found to be avid DNA binders with binding affinity either comparable or better than existing copper(II)–polypyridyl-based artificial nucleases.^{41–46} Binding characteristics favoured a groove/partial intercalative mode for interacting with DNA, while nuclease activity appeared efficient under chemical as well as light stimulus. It is concluded that peripheral ligand architecture influences the extent of DNA binding and cleavage activity, where more planar, hydrophobic and aromatic ligands appeared to be more effective DNA binders as well as cleavers under chemical or light stimulus. Apparently, molecular docking studies correlated well with the experimental evidence and favoured the DNA binding trends as observed.

Experimental section

Materials and methods

Copper(II) perchlorate hexahydrate, 2-acetyl pyridine, polyethylene glycol (PEG-300), 4-pyridine carboxaldehyde, 2-naphthaldehyde, 9-anthraldehyde, 1-pyrene carbaldehyde, 1,10-phenanthroline monohydrate, potassium tert. butoxide, sodium perchlorate, tetrabutylammonium perchlorate (TBAP), 3-mercaptopropionic acid (3-MPA), ethylenediaminetetraacetic acid (EDTA) and tris-HCl base were purchased from Sigma-Aldrich and used as received. Sodium hydroxide, ethidium bromide (EB), ammonium acetate, aqueous ammonia, and sodium sulphate were purchased from SD Fine Chemicals, India and used as received. All solvents, *viz.* ethanol, methanol, dichloromethane, and chloroform, were purchased from Rankem, India and were distilled and degassed following established procedures and kept in an N₂-filled glovebox (O₂ < 0.5 ppm). Ultra-pure Milli-Q water ($\rho = 18.2 \text{ M}\Omega \text{ cm}$ at 25 °C) was used in all experiments. A 1 mg mL⁻¹ solution of calf thymus DNA (ct-DNA) and a 250 μg mL⁻¹ solution of pUC19

DNA was procured from Genei, Bangalore, and kept at –20 °C inside an N₂ filled glovebox.

Physical characterization

Optical measurements. All UV/vis spectra were recorded on a JASCO UV-vis-NIR spectrophotometer (Model V-670). For measurements, a pair of quartz cuvettes with an optical path length of 1 cm was used. Every measurement and DNA binding studies were performed at room temperature and suitable baselines were recorded for preliminary adjustments. A Perkin Elmer fluorescence spectrometer (Model LS45) was employed for carrying out competitive DNA binding studies with a quartz cuvette with an optical path length of 1 cm. Thermal denaturation studies were performed on a Perkin Elmer UV/vis spectrophotometer (Model Lambda 45) equipped with a Peltier temperature-controlling programmer (PTP-6) functionality and a water circulation system. A Thermo Scientific NanoDrop 2000 spectrophotometer was used for determining DNA purity. A JASCO circular dichroism spectropolarimeter (Model J-815) was used for determining structural changes in DNA upon DNA binding with copper complexes. A quartz cuvette with a 1 cm path length was used for carrying out measurements with proper preliminary adjustments.

Electrochemical measurements. All cyclic voltammograms were recorded on a CH Instruments electrochemical workstation (Model 660D). A single-compartment cell with a three-electrode setup was used to perform the experiments. A glassy carbon electrode, a Pt wire and an Ag/AgCl electrode (3 M KCl) were used as working, counter and reference electrode respectively. TBAP (tetra butyl ammonium perchlorate) (0.1 M) was used as supporting electrolyte. Complex solutions (1 mM in 30% DMF) were bubbled with N₂ gas for ~20 min prior to recording cyclic voltammograms.

Electron paramagnetic resonance measurements. EPR measurements were carried out on a JEOL JES-FA series EPR spectrometer. All measurements were carried out in DMF at 77K (DMF glass) with 2,2-diphenyl-1-picrylhydrazyl (DPPH) as an internal standard. The instrument was operated at X-band frequencies (9.1 GHz) and a 100 kHz field.

Nuclear magnetic resonance measurements. All ¹H-NMR spectra were recorded on a JEOL JNMECX 400p spectrometer at room temperature using a suitable deuterated solvent. All chemical shifts (δ) were recorded in ppm with reference to tetramethylsilane (TMS), and coupling constant (J) values are provided in Hz.

Density functional studies. The ground state geometry optimizations of TPYC-1 to 4 were carried out in the gas phase using the B3LYP method.^{47,48} The LANL2DZ basis set with effective core potential was used for the copper atom. The 6-31G* basis set was used for carbon, hydrogen and nitrogen atoms.⁴⁹ The initial geometry was obtained from the standard geometrical parameters. All calculations were performed using the Gaussian 09 program package.⁵⁰

Conflicts of interest

The authors declare no competing or financial conflict.

Acknowledgements

This work was financially supported by the University Grants Commission (F-37-407/2009(SR)), New Delhi, India. VS thanks University Grants Commission (UGC), India for a Senior Research Fellowship. RDG thanks the Department of Science and Technology (SERB/F/1448/2012-13).

Notes and references

- 1 F. H. Westheimer, *Science*, 1987, **235**, 1173–1178.
- 2 J. Hormann, C. Perera, N. Deibel, D. Lentz, B. Sarkar and N. Kulak, *Dalton Trans.*, 2013, **42**, 4357–4360.
- 3 J. C. Wang, *Nat. Rev. Mol. Cell Biol.*, 2002, **3**, 430–440.
- 4 S. Lee, S.-R. Jung, K. Heo, J. A. W. Byl, J. E. Deweese, N. Osheroff and S. Hohng, *Proc. Natl. Acad. Sci. U. S. A.*, 2012, **109**, 2925–2930.
- 5 H. W. Boyer, *Annu. Rev. Microbiol.*, 1971, **25**, 153–176.
- 6 J. E. Deweese and N. Osheroff, *Nucleic Acids Res.*, 2009, **37**, 738–748.
- 7 C. Hélène, N. T. Thuong, T. Saison-Behmoaras and J.-C. François, *Trends Biotechnol.*, 1989, **7**, 310–315.
- 8 F. Mancin, P. Scrimin, P. Tecilla and U. Tonellato, *Chem. Commun.*, 2005, 2540–2548.
- 9 T. I. Cornu, S. Thibodeau-Beganny, E. Guhl, S. Alwin, M. Eichtinger, J. Joung and T. Cathomen, *Mol. Ther.*, 2008, **16**, 352–358.
- 10 S. Aoki and E. Kimura, *Chem. Rev.*, 2004, **104**, 769–788.
- 11 S. E. Wolkenberg and D. L. Boger, *Chem. Rev.*, 2002, **102**, 2477–2496.
- 12 J. D. West and L. J. Marnett, *Chem. Res. Toxicol.*, 2006, **19**, 173–194.
- 13 M. J. Clarke, *Coord. Chem. Rev.*, 2003, **236**, 209–233.
- 14 M. C. DeRosa and R. J. Crutchley, *Coord. Chem. Rev.*, 2002, **233**, 351–371.
- 15 J. L. Sessler, G. Hemmi, T. D. Mody, T. Murai, A. Burrell and S. W. Young, *Acc. Chem. Res.*, 1994, **27**, 43–50.
- 16 M. Ochsner, *J. Photochem. Photobiol., B*, 1996, **32**, 3–9.
- 17 K. K. Patel, E. A. Plummer, M. Darwish, A. Rodger and M. J. Hannon, *J. Inorg. Biochem.*, 2002, **91**, 220–229.
- 18 K. Suntharalingam, D. J. Hunt, A. A. Duarte, A. J. White, D. J. Mann and R. Vilar, *Chem. – Eur. J.*, 2012, **18**, 15133–15141.
- 19 V. Singh, P. C. Mondal, A. Kumar, Y. L. Jeyachandran, S. K. Awasthi, R. D. Gupta and M. Zharnikov, *Chem. Commun.*, 2014, **50**, 11484–11487.
- 20 K. Abdi, H. Hadadzadeh, M. Weil and H. A. Rudbari, *Inorg. Chim. Acta*, 2014, **416**, 109–121.
- 21 A. J. Bard, L. R. Faulkner, J. Leddy and C. G. Zoski, *Electrochemical Methods: Fundamentals and Applications*, Wiley, New York, 1980.
- 22 J.-Y. Go and S.-I. Pyun, *J. Solid State Electrochem.*, 2007, **11**, 323–334.
- 23 E. Garribba and G. Micera, *J. Chem. Educ.*, 2006, **83**, 1229.
- 24 J. Eisenstein, *J. Chem. Phys.*, 1958, **28**, 323–329.
- 25 M. Murali, M. Palaniandavar and T. Pandiyan, *Inorg. Chim. Acta*, 1994, **224**, 19–25.
- 26 J. Peisach and W. Blumberg, *Arch. Biochem. Biophys.*, 1974, **165**, 691–708.
- 27 F. A. Chavez, M. M. Olmstead and P. K. Mascharak, *Inorg. Chem.*, 1996, **35**, 1410–1412.
- 28 R. C. Chikate, A. R. Belapure, S. B. Padhye and D. X. West, *Polyhedron*, 2005, **24**, 889–899.
- 29 P. Bindu, M. R. P. Kurup and T. R. Satyakeerty, *Polyhedron*, 1998, **18**, 321–331.
- 30 R. Neiman and D. Kivelson, *J. Chem. Phys.*, 1961, **35**, 156–161.
- 31 V. Uma, M. Kanthimathi, J. Subramanian and B. U. Nair, *Biochim. Biophys. Acta, Gen. Subj.*, 2006, **1760**, 814–819.
- 32 M.-J. Fernández, B. Wilson, M. Palacios, M.-M. Rodrigo, K. B. Grant and A. Lorente, *Bioconjugate Chem.*, 2007, **18**, 121–129.
- 33 E. T. Kool, *Chem. Rev.*, 1997, **97**, 1473–1488.
- 34 A. Paul and S. Bhattacharya, *Curr. Sci.*, 2012, **102**, 212–231.
- 35 C. Hiort, B. Norden and A. Rodger, *J. Am. Chem. Soc.*, 1990, **112**, 1971–1982.
- 36 H.-C. Becker and B. Nordén, *J. Am. Chem. Soc.*, 1997, **119**, 5798–5803.
- 37 P. U. Maheswari and M. Palaniandavar, *J. Inorg. Biochem.*, 2004, **98**, 219–230.
- 38 K. Fukui, *Physiology or Medicine Literature Peace Economic Sciences*, 1992, p. 9.
- 39 J. Bernadou, G. Pratviel, F. Bennis, M. Girardet and B. Meunier, *Biochemistry*, 1989, **28**, 7268–7275.
- 40 J. F. Michalec, S. A. Bejune, D. G. Cuttall, G. C. Summerton, J. A. Gertenbach, J. S. Field, R. J. Haines and D. R. McMillin, *Inorg. Chem.*, 2001, **40**, 2193–2200.
- 41 V. Uma, M. Elango and B. U. Nair, *Eur. J. Inorg. Chem.*, 2007, 3484–3490.
- 42 S. Rajalakshmi, T. Weyhermüller, M. Dinesh and B. U. Nair, *J. Inorg. Biochem.*, 2012, **117**, 48–59.
- 43 T. K. Goswami, S. Gadadhar, M. Roy, M. Nethaji, A. A. Karande and A. R. Chakravarty, *Organometallics*, 2012, **31**, 3010–3021.
- 44 V. M. Manikandamathavan, R. P. Parameswari, T. Weyhermüller, H. R. Vasanthi and B. U. Nair, *Eur. J. Med. Chem.*, 2011, **46**, 4537–4547.
- 45 V. Uma, M. Kanthimathi, T. Weyhermüller and B. U. Nair, *J. Inorg. Biochem.*, 2005, **99**, 2299–2307.
- 46 A. Kumar, J. P. Chinta, A. K. Ajay, M. K. Bhat and C. P. Rao, *Dalton Trans.*, 2011, **40**, 10865–10872.
- 47 M. M. Francl, W. J. Pietro, W. J. Hehre, J. S. Binkley, M. S. Gordon, D. J. DeFrees and J. A. Pople, *J. Chem. Phys.*, 1982, **77**, 3654–3665.
- 48 V. A. Rassolov, M. A. Ratner, J. A. Pople, P. C. Redfern and L. A. Curtiss, *J. Comput. Chem.*, 2001, **22**, 976–984.
- 49 W. R. Wadt and P. J. Hay, *J. Chem. Phys.*, 1985, **82**, 284–298.
- 50 M. J. Frisch, G. W. Trucks, H. B. Schlegel, G. E. Scuseria, M. A. Robb, J. R. Cheeseman, J. A. Montgomery Jr., T. Vreven, K. N. Kudin, J. C. Burant, J. M. Millam, S. S. Iyengar, J. Tomasi, V. Barone, B. Mennucci, M. Cossi, G. Scalmani, N. Rega, G. A. Petersson, H. Nakatsuji, M. Hada, M. Ehara,

K. Toyota, R. Fukuda, J. Hasegawa, M. Ishida, T. Nakajima, Y. Honda, O. Kitao, H. Nakai, M. Klene, X. Li, J. E. Knox, H. P. Hratchian, J. B. Cross, C. Adamo, J. Jaramillo, R. Gomperts, R. E. Stratmann, O. Yazyev, A. J. Austin, R. Cammi, C. Pomelli, J. W. Ochterski, P. Y. Ayala, K. Morokuma, G. A. Voth, P. Salvador, J. J. Dannenberg, V. G. Zakrzewski, S. Dapprich, A. D. Daniels, M. C. Strain,

O. Farkas, D. K. Malick, A. D. Rabuck, K. Raghavachari, J. B. Foresman, J. V. Ortiz, Q. Cui, A. G. Baboul, S. Clifford, J. Cioslowski, B. B. Stefanov, G. Liu, A. Liashenko, P. Piskorz, I. Komaromi, R. L. Martin, D. J. Fox, T. Keith, M. A. Al-Laham, C. Y. Peng, A. Nanayakkara, M. Challacombe, P. M. W. Gill, B. Johnson, W. Chen, M. W. Wong, C. Gonzalez and J. A. Pople, *Gaussian 03, Revision B.03*, Gaussian, Inc., Pittsburgh, PA, 2003.